Humidity- and Sunlight-Driven Motion of Chemically Bonded Polymer Bilayer with Programmable Surface Patterns

Lidong Zhang,* Xiaxin Qiu, Yihui Yuan, Ting Zhang

Department of Chemistry and Molecular Engineering, East China Normal University, Shanghai, 200241, People's Republic of China

E-mail:ldzhang@chem.ecnu.edu.cn

*Corresponding author: Lidong Zhang: E-mail:ldzhang@chem.ecnu.edu.cn

ORCID: Lidong Zhang: 0000-0002-0501-6162

Supplementary Figures

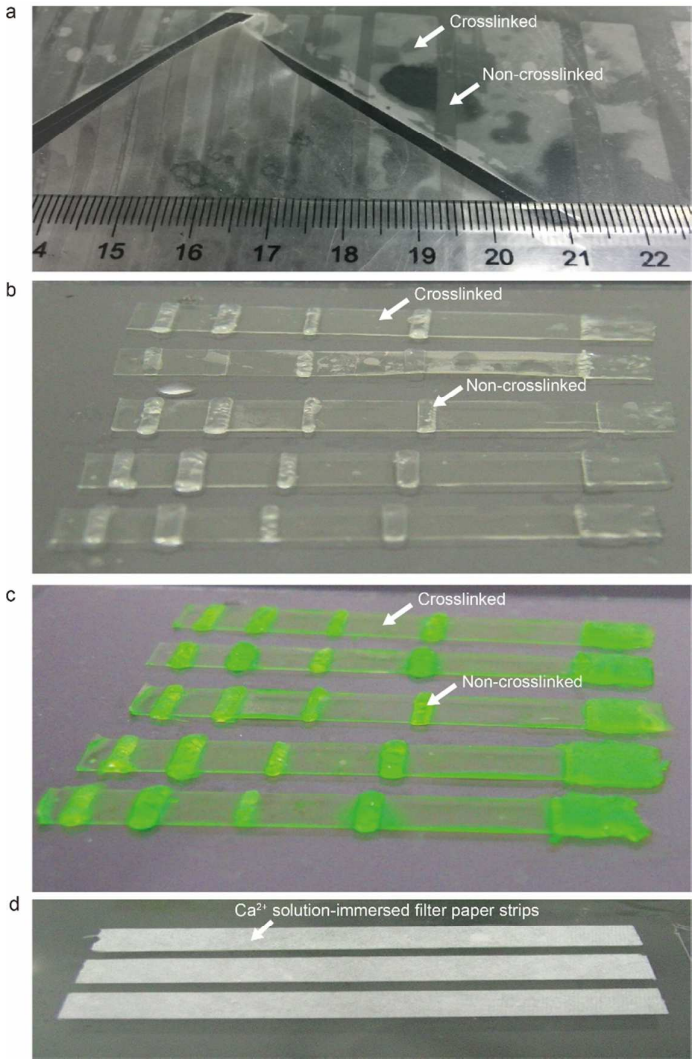

Figure S1. Crosslinking-patterned bilayer films of SA/PVDF. (a) Photograph of the SA/PVDF bilayer, showing crosslinked and non-crosslinked patterns on SA side before water sorption. (b) The strips of SA/PVDF bilayers indicating different water sorption abilities between crosslinked and non-crosslinked patterns on SA side. (c) The strips were stained with dye for better observation. (d) Ca^{2+} solution-immersed filter paper strips covered on the bilayer of SA/PVDF, demonstrating how to make crosslinking patterns on SA side.

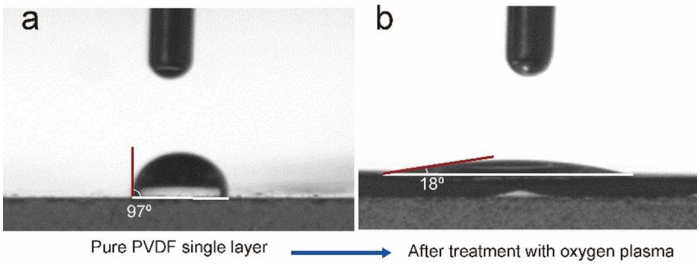

Figure S2. Contact angles of the bare and modified PVDF surfaces. (a) The pure PVDF has a hydrophobic surface with a contact angle of 97°, and (b) it becomes hydrophilic with the contact angle changing to 18° after treatment by oxygen plasma for 5 min.

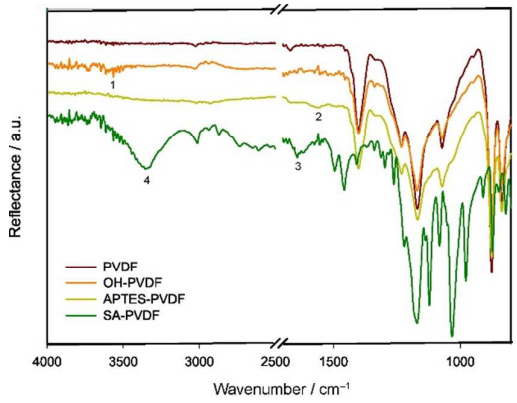

Figure S3. ATR-IR spectra of bare and modified PVDF surfaces. Characteristic peaks are assigned in numbers from 1 to 4. Very weak peak 1 represents hydroxyl groups generated on PVDF surface after treatment with oxygen plasma. Peak 2 indicates the primary amine groups formed by incubation of OH-PVDF in APTES. Peak 3 and 4 represent the amide bond coupling of alginate and multiple hydroxyl groups of alginate, respectively.

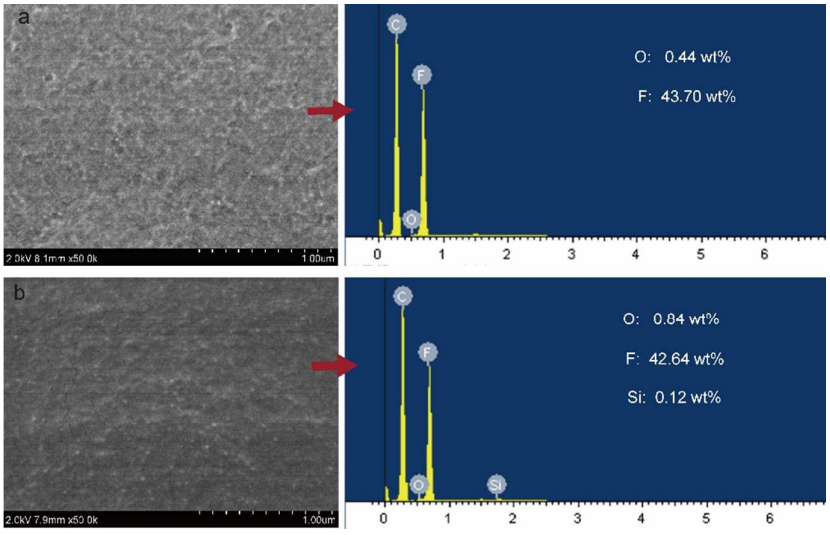

Figure S4. Scanning electron microscope (SEM) images and energy dispersive X-Ray spectroscopy (EDX) of modified PVDF surfaces. (a) After oxygen plasma treatment for 5 min, the oxygen atom content on the PVDF surface gets up to 0.44 wt% indicating the formation of hydroxyl groups on the film surface (marked as OH-PVDF), and (b) after incubation of OH-PVDF in APTES, the oxygen atom content inreased to 0.84 wt% and the silicon atom was detected to be 0.12 wt%, which implied the successful introduction of APTES on the surface.

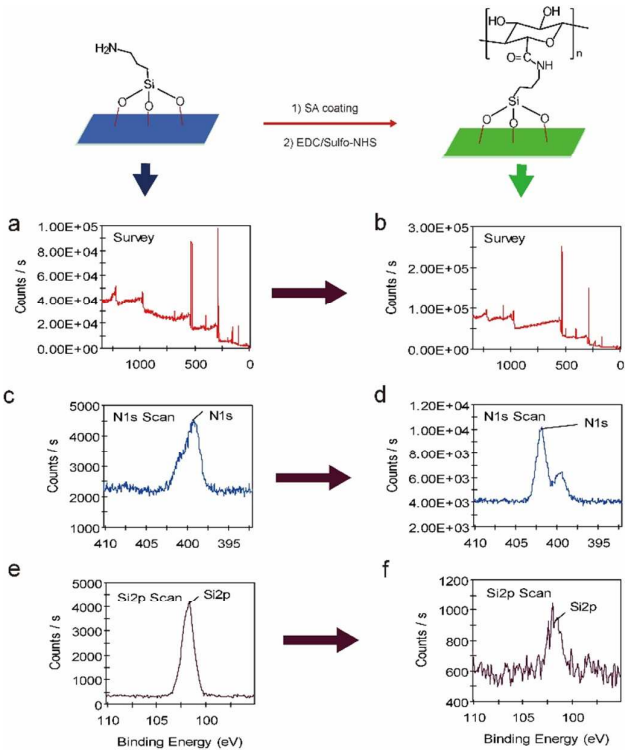

Figure S5. X-ray photoelectron spectroscopy (XPS). (a,b) Survey scans of APTES-modified PVDF and SA-modified PVDF. (c,d) Typical N1s scans and (e,f) typical Si2p scans for APTES-modified PVDF side and SA-modified PVDF side, repectively.

Peak table 1. XPS scans for APTES-modified PVDF side.

Name	Start BE	Peak BE	End BE	Height CPS	FWHM eV	Area (P) CPS.eV	Area (N) TPP-2M	Atomic %
Si2p	109.98	101.78	95.18	3735.44	1.4	6190.99	0.08	10.44
C1s	297.98	284.36	279.18	22568.41	1.33	39715.5	0.5	63.3
N1s	410.03	399.24	392.13	2295.12	2.48	6648.97	0.05	6.56
O1s	544.98	531.73	525.18	18276.33	1.47	32716.25	0.16	19.7

Peak table 2. XPS scans for SA-modified PVDF side.

Name	Start BE	Peak BE	End BE	Height CPS	FWHM eV	Area (P) CPS.eV	Area (N) TPP-2M	Atomic %
Si2p	109.98	101.79	95.18	415.78	1.73	1312.41	0.02	1.08
C1s	297.98	286.07	279.18	28781.25	1.59	76567.05	0.97	59.43
N1s	410.03	401.88	392.13	6043.49	1.36	13937.81	0.11	6.69
O1s	544.98	531.7	525.18	40485.29	2.63	111892.52	0.53	32.8

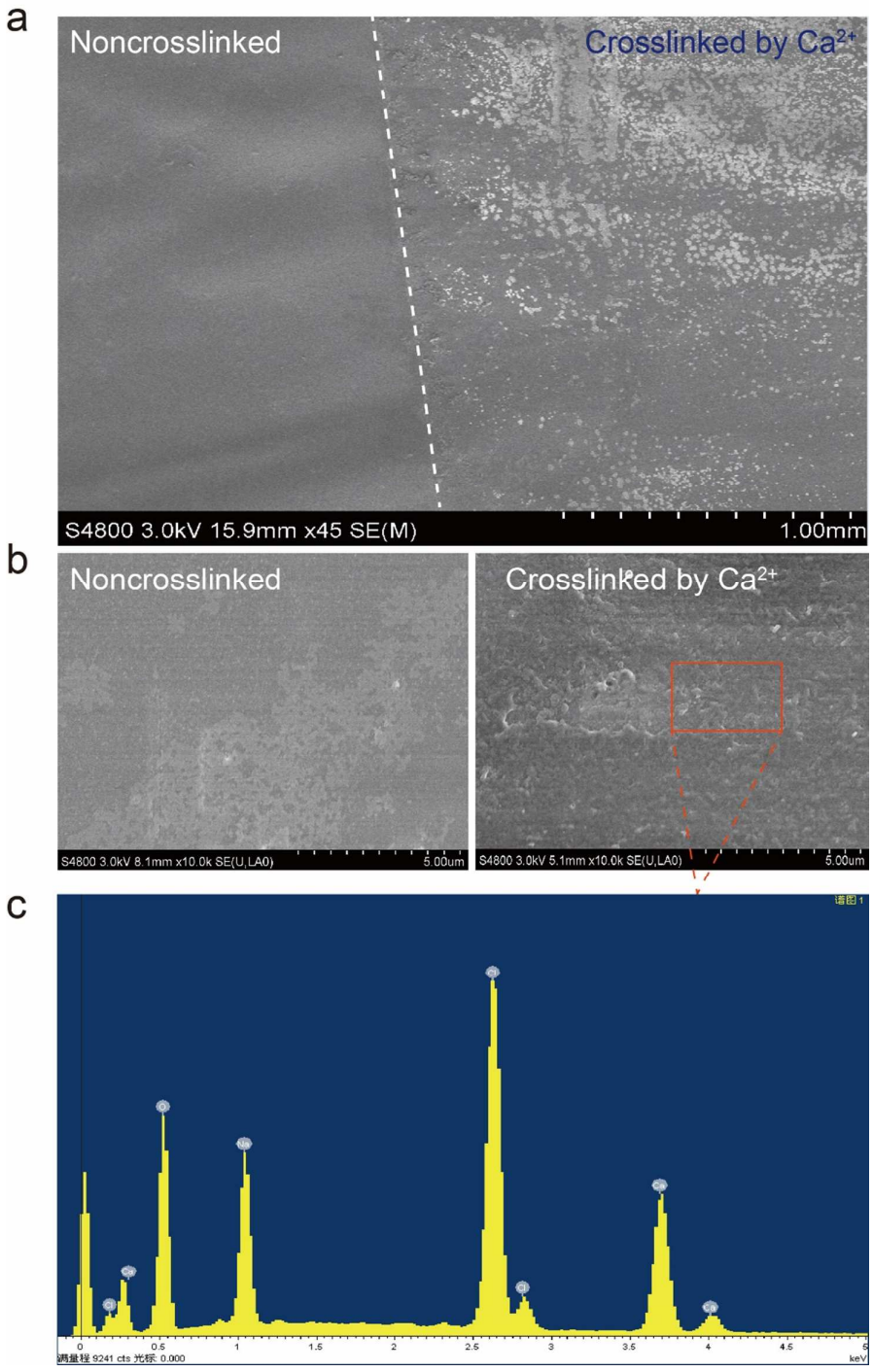

Figure S6. (a) Scanning electron microscope (SEM) images of the SA film, showing the surface morphologies of non-crosslinked and crosslinked regions. (b) Magnified observation of the surface morphologies of non-crosslinked and crosslinked regions in the SA film. (c) Energy dispersive X-Ray spectroscopy for crosslinked regions, to detect the calcium ion in the SA film.

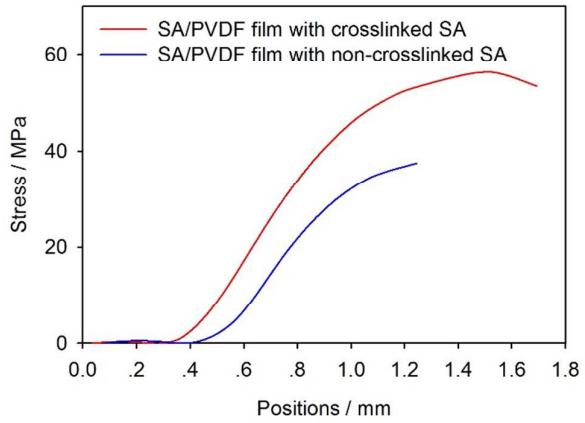

Figure S7. Mechanical test of the SA/PVDF film before and after crosslinking reaction at SA layer. After crosslinking for the SA layer, the bilayer of SA/PVDF has higher mechnical stress.

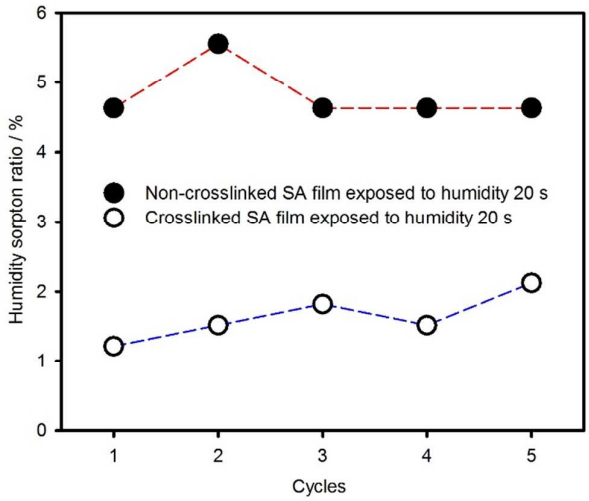

Figure S8. Examination of the humidity-sorption abilities of SA films before and after crosslinking by Ca^{2+}. A certain amount of dried SA film (recorded as M_0) was placed on a most filter paper for humidity sorption 20 s, and the weight was measured as M_s. The humidity sorption ratio was calculated as: $(M_s - M_0) \times 100\% / M_0$. This process was repeated five times. The results indicate that the non-crosslinked SA film has higher humidity sorption ability than the crosslinked SA film in the same time course.

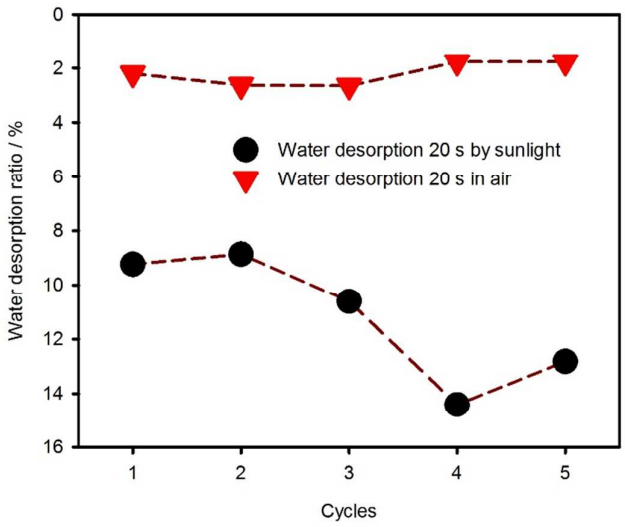

Figure S9. Examination of the humidity desorption abilities of non-crosslinked SA film. A certain amount of dried SA film was placed on a most filter paper for humidity sorption 20 s, and the weight was measured as M_s. The humidity-treated film was then moved to a dry substrate to allow humidity desorption in air at 23°C or with irradiation of sunlight for 20 s, and the weight of the film was measured as M_d. The humidity desorption ratio was calculated as: $(M_s - M_d) \times 100\% / M_s$. This process was repeated five times. The results indicate that the non-crosslinked SA film desorbed water molecules faster when irradiated with sunlight.

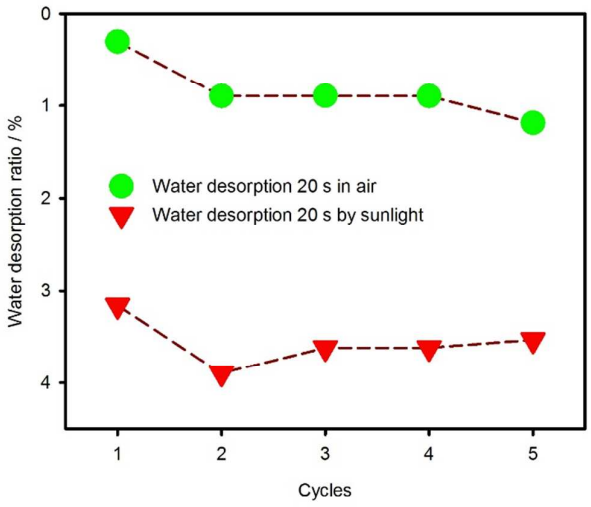

Figure S10. Examination of the humidity desorption abilities of crosslinked SA film. The testing processes were same as in Figure S2. The results also indicate that the sunlight irradiation can dramatically accelerate water desorption of the film. On the other hand, after crosslinking by Ca^{2+}, the SA film has lower humidity de/sorption abilities, implying lower humidity sensitivity in the crosslinked SA film.

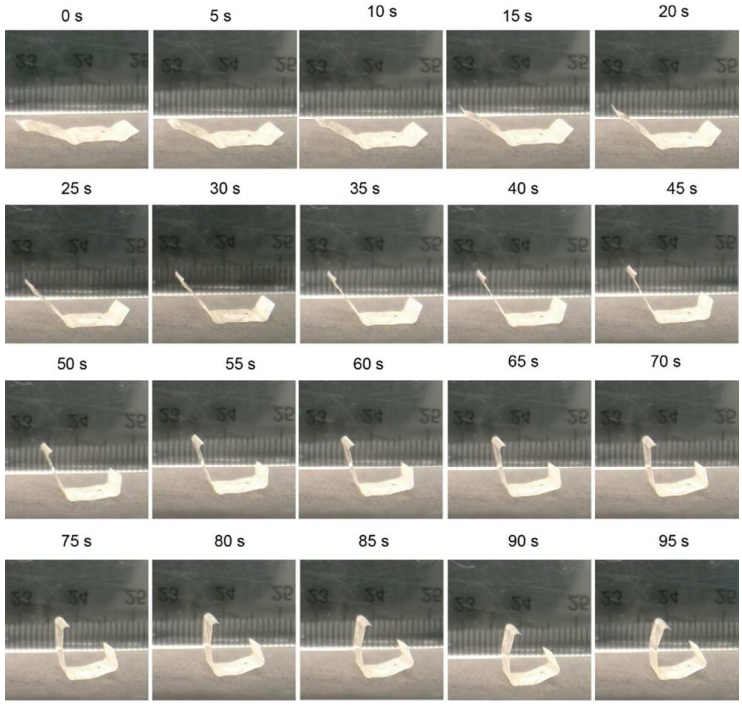

Figure S11. Snapshots of the bilayer of SA/PVDF slowly bending to SA side along the non-crosslinked pattern by dehydration-induced contraction on a dry substrate at 26 °C,

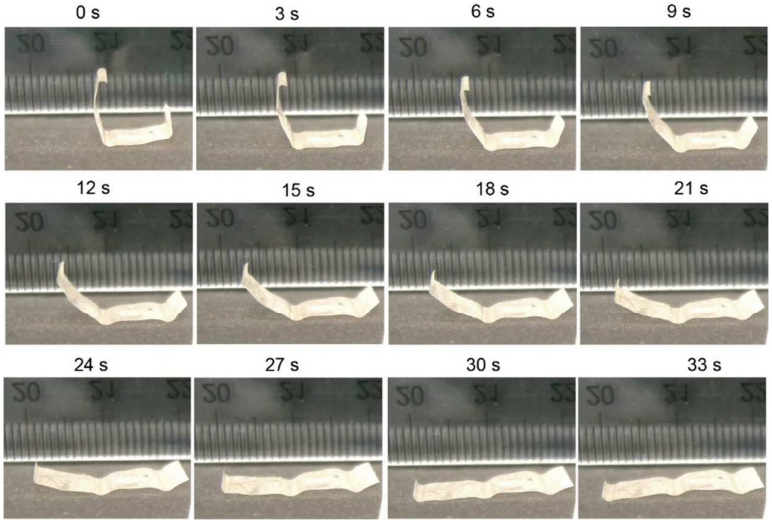

Figure S12. Snapshots of the bended bilayer of SA/PVDF slowly bending back to original flat shape by hydration on a moist substrate at 23 °C.

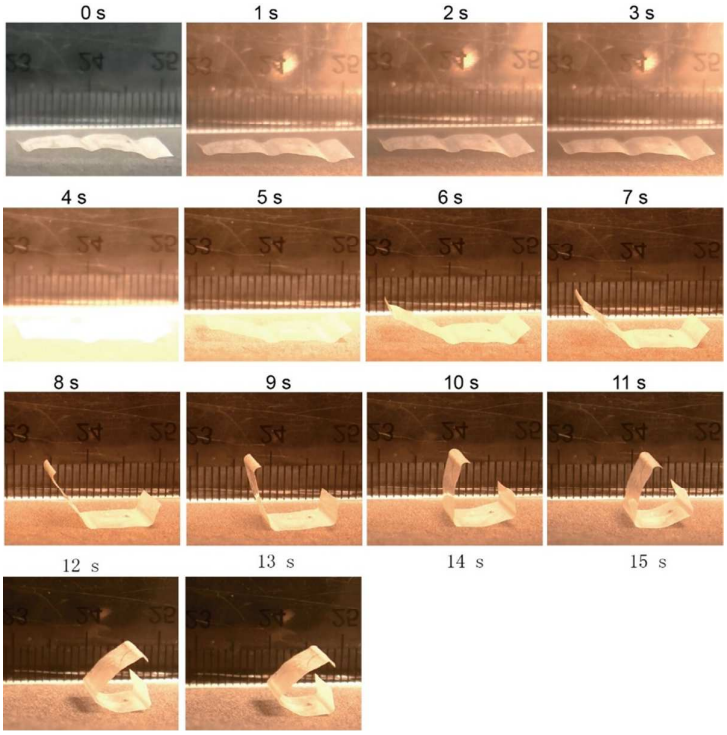

Figure S13. Snapshots of the bilayer of SA/PVDF quickly bending to SA side along the non-crosslinked pattern by dehydration-induced contraction with sunlight at 115 mW cm^{-2}.

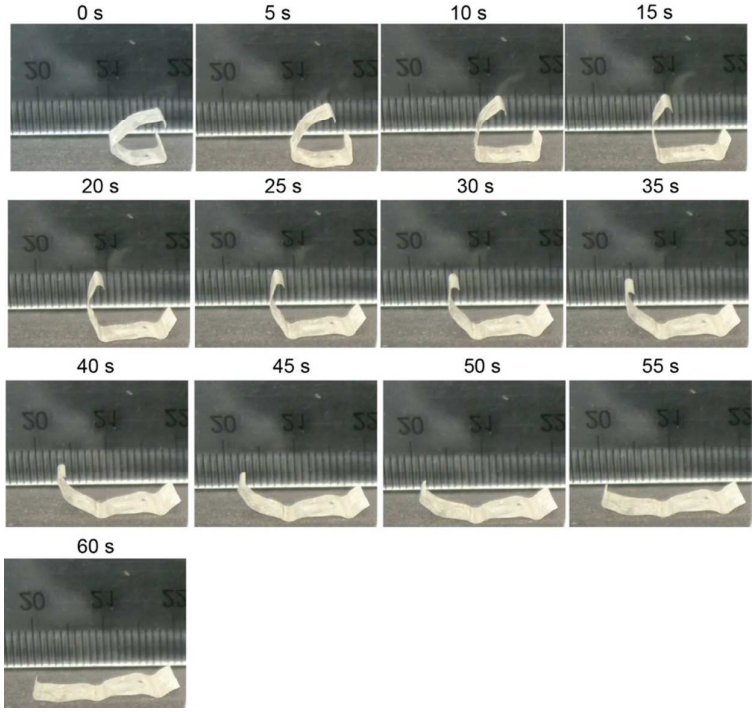

Figure S14. Snapshots of the sunlight-bended bilayer of SA/PVDF bending back to original flat shape by rehydration on a moist substrate at 23 °C.

Figure S15. Thermal infrared images of SA/PVDF bilayer (thermal infrared camera, FLIR C2). The non-crosslinked patterns aligned at +30° to the long axis of the strip that induces the strip to twist into a left-handed helix by desorption of water on a dry substrate.

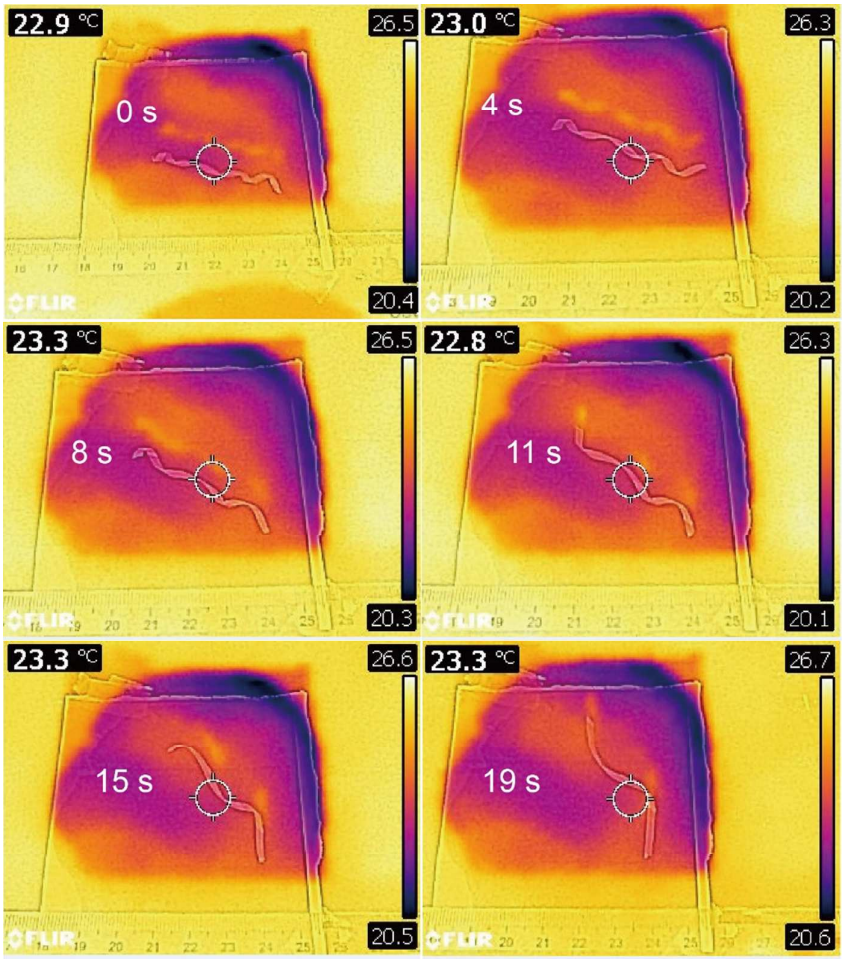

Figure S16. Thermal infrared images of SA/PVDF bilayer. The left-handed helix formed in Figure S11, untwists by water sorption on a moist substrate (Filter paper containing ~30wt% of water).

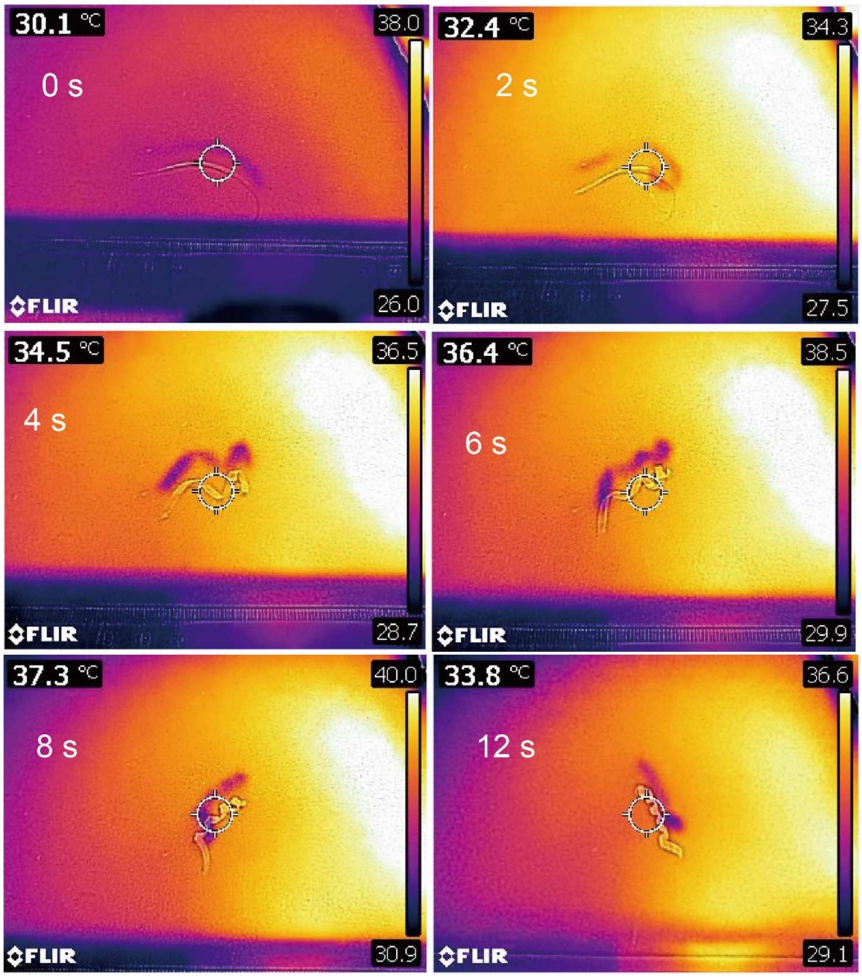

Figure S17. Thermal infrared images of SAPVDF bilayer. The bilayer strip with non-crosslinked patterns aligned at +30° to the long axis, twists into a left-handed helix while irradiated with sunlight at 115 mW cm^{-2}.

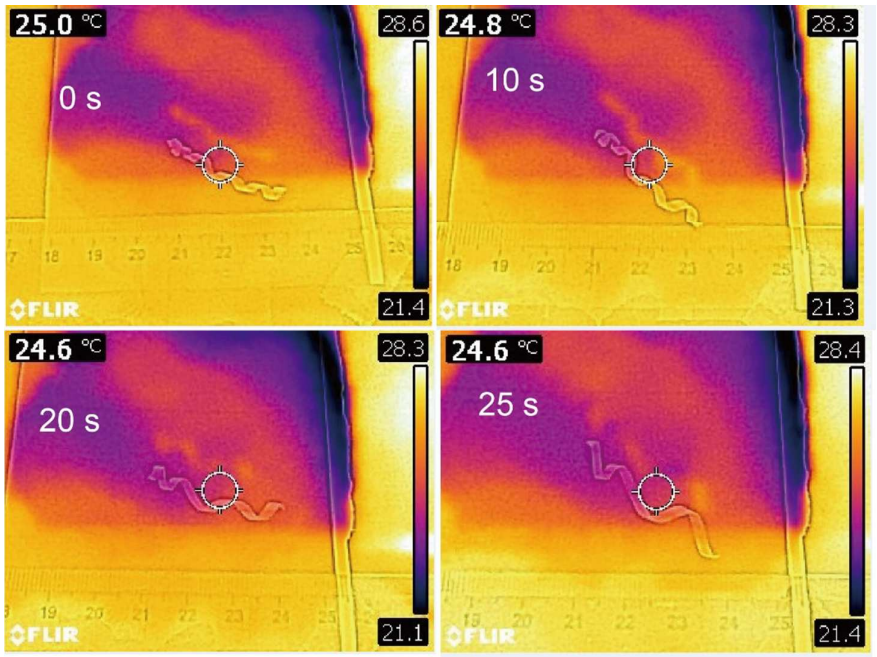

Figure S18. Thermal infrared images of SA/PVDF bilayer. The left-handed helix formed in Figure S13, untwists by adsorption of water on a moist substrate (Filter paper containing ~30wt% of water).

Legends for Supplementary Movies

Movie S1. Peeling process of physically-combined SA/PVDF bilayer that is easily separated from each other.

Movie S2. Peeling process of chemically-combined SA/PVDF bilayer that is hard separated from each other.

Movie S3. Crosslinking-patterned chemically-combined SA/PVDF bilayer folds up by sunlight, while crosslinking-patterned single SA bilayer doesn't have apparent folding response to sunlight.

Movie S4. Crosslinking-patterned chemically-combined SA/PVDF bilayer deforms from irregular status to regular shape by sunlight.

Movie S5. Twisting of chemically-combined SA/PVDF bilayer along non-crosslinking-pattern driven by sunlight.

Movie S6. Left-handed twisting/untwisting of the chemically-combined SA/PVDF bilayer by sunlight and humidity, in which the crosslinked/non-crosslinked patterns aligned at the angle of +30° to the long axis. The video is shown at four times the real speed.

Movie S7. Right-handed twisting/untwisting of the chemically-combined SA/PVDF bilayer by sunlight and humidity, in which the crosslinked/non-crosslinked patterns aligned at the angle of −30° to the long axis. The video is shown at four times the real speed.

Movie S8. Cross-shaped bilayer folds up along the non-crosslinked patterns only, indicating excellent controllability of the patterns over the shape change.

Movie S9. Mimetic motion of the crosslinking-patterned chemically-combined SA/PVDF bilayer, resembling the behaviors of a caterpillar. The video is shown at three times the real speed.